

# Towards Trapped-Ion Thermometry Using Cavity-Based EIT

Abhijit Kundu,<sup>1</sup> Vijay Bhatt,<sup>1</sup> and Arijit Sharma<sup>1, 2, \*</sup>

<sup>1</sup>*Department of Physics, Indian Institute of Technology Tirupati, Yerpedu-517619, Andhra Pradesh, India.*

<sup>2</sup>*Center for Atomic, Molecular, and Optical Sciences and Technologies,  
Indian Institute of Technology Tirupati, Yerpedu-517619, Andhra Pradesh, India.*

(Dated: February 16, 2026)

We present a technique for measuring ion temperature using cavity-based electromagnetically induced transparency (EIT) applicable for cavity-QED systems in the strong coupling regime. This method enables efficient extraction of the ion's phonon occupation number following sub-Doppler cooling close to the motional ground state. The proposed method relies on monitoring the cavity probe transmission while scanning the probe laser frequency once cavity EIT is established using the control beam, significantly simplifying the measurement procedure. We theoretically establish a model that demonstrates influence of thermal state of the trapped ion via the EIT linewidth measured. We show how the cavity EIT transmission may be used as a thermometry tool to deduce the ion temperature as well as the motional state for an ion in the sub-Doppler cooling regime. The current method can only be used for operation in the resolved-sideband regime, where individual motional states can be selectively addressed for all relevant transitions either by selecting appropriate energy levels for the three-level system or by employing strong confinement with high secular frequencies ( $\sim 10\text{MHz}$ ).

## I. INTRODUCTION

Trapped ions offer a well-controlled platform for precision metrology, cavity quantum electrodynamics (QED), and quantum information processing due to their long coherence time and exceptional degree of experimental controllability [1–4].

Achieving and confirming near-ground-state cooling is essential, since even a small residual motional excitation can degrade coherence and reduce the fidelity of quantum operations [5, 6]. With successful demonstrations across a broad range of ion species and trap architectures, resolved sideband cooling has emerged as the standard technique for preparing trapped ions close to the motional ground state [5, 7, 8]. For this reason, accurate thermometry after sideband cooling is crucial for describing cooling performance and validating subsequent quantum operations. After compensation of excess micromotion, it is possible to characterize the motion of a trapped ion in a radio-frequency Paul trap [5]. Ion temperature is directly determined by a discrete phonon occupation number that characterizes the motional state. Determining this phonon occupation provides a crucial bench-

mark for coherent quantum operations and enables a direct evaluation of the ions' thermal state [1, 5, 9].

A variety of techniques have been developed to deduce the motional occupation of trapped ions [9–11]. The most popular method is resolved sideband thermometry, which assumes a thermal motional distribution and uses the ratio of red to blue sideband transition strengths to estimate the mean phonon number [7, 12]. More generally, reconstruction techniques that do not strictly rely on thermal assumptions are made possible by extracting phonon distribution information from Rabi oscillations in carrier and sideband transitions [9–11]. These methods are well known and typically require precise internal-state preparation and the detection of projective states.

There has been a growing interest in cavity quantum electrodynamics with trapped ions due to its potential to realize scalable quantum networks, enhanced light-matter coupling, and effective ion-photon interfaces [13–19]. Interference-based phenomena such as cavity-assisted electromagnetic-induced transparency (EIT) are made possible by the presence of an optical cavity, which alters the interaction between the ion and the electromagnetic field. Since its discovery, EIT [20] has made it possible for a wide range of coherent optical

\* arijit@iittp.ac.in

control applications, such as slow light in atomic medium [21], quantum memory [22], laser cooling [23], precision spectroscopy, and sensing [13].

Cavity-based EIT has been studied in a number of regimes to enable features such as narrowing of the cavity linewidth and enhanced optical nonlinearities [16, 17, 24]. A key feature of cavity-induced EIT is its sensitivity to decoherence mechanisms in the coupled ion-cavity system. Coupling to vibrational sidebands causes phonon-dependent dephasing of the effective  $\Lambda$ -type system in the presence of motional excitation, changing the coherence and causing the EIT interference [23, 25]. The cavity-EIT transparency window is thus systematically expanded by thermal phonons. Thermally induced fluctuations alter the effective decoherence rates in the presence of motional excitation which affects the EIT transparency features' width and shape. This dependence suggests that the cavity-EIT can serve as an indirect probe of the ion's motional temperature.

In this paper, we theoretically investigate a cavity-enhanced thermometry scheme for trapped ions that exploits this phonon-induced modification of cavity-induced EIT. By including vibrational sidebands and the ion's motion coupled to a thermal reservoir in a  $\Lambda$ -type ion-cavity setup, we demonstrate that the phonon occupation of the trapped ion systematically affects the linewidth of the cavity-EIT resonance. This dependence can be used as a direct probe of the mean phonon number by tuning the coupling field to motional sideband transitions. Therefore, the suggested method offers a cavity-compatible thermometry technique that does not depend on projective state detection after sideband cooling. In this theoretical framework a direct link between measurable modification of the cavity-EIT resonance and motional decoherence induced by thermal phonon is established. This enhances current thermometry methods and offers an experimentally feasible path for temperature diagnostics in trapped-ion cavity-QED systems.

We show that the coupling laser causes a

phonon number-dependent change in the effective Rabi frequency when it is tuned to motional sideband transition. This results in a systematic and temperature-dependent broadening of the cavity-EIT feature. We determine a quantitative relationship between the measured cavity-EIT linewidth and the ion temperature by numerically solving the complete open-system dynamics, which includes cavity loss, spontaneous emission, and phonon damping caused by a thermal reservoir. Our results indicate that this technique allows for precise thermometry in the resolved-sideband and sub-Doppler regimes and can be expanded to parameter regimes that are consistent with experimentally realized strong coupling ion-cavity systems[16–19].

In this work a direct link between motional decoherence and cavity transmission properties is established, and a cavity-compatible minimally invasive thermometry method for trapped ions is presented. Beyond thermometry, the shown sensitivity of cavity-EIT to the motional state of the ion creates new opportunities for studying measurement-induced back-action in cavity-QED systems and for ongoing heating dynamics monitoring.

The paper is organized as follows: In section II, we present the theoretical model and Hamiltonian including the treatment of ion motion and dissipative processes. In section III, numerical results for linewidth extraction and cavity transmission are shown. The section IV examines how phonons affect the cavity-EIT spectrum. The analysis of ion temperature and the role of thermalization dynamics are discussed in section V. Finally, a summary of the key results and concluding remarks are given in section section VII.

## II. THEORY AND MODEL

Cavity-EIT systems have been extensively studied in the literature [16, 17, 24, 26–30]. These studies demonstrate that the cavity out-

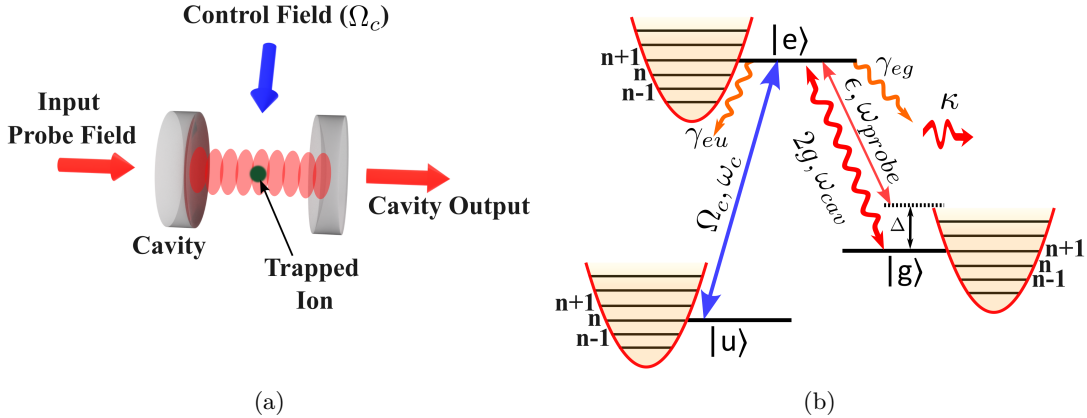


FIG. 1: (a) Schematic of the cavity-based electromagnetically induced transparency (EIT) configuration, where a trapped ion interacts with a single cavity mode. (b) Energy-level diagram of the cavity-EIT scheme including vibrational states. The coupling laser drives the  $|u\rangle \rightarrow |e\rangle$  transition with the addition of one vibrational quantum, while spontaneous decay to  $|g\rangle$  preserves the vibrational level. The probe field and cavity mode couple the  $|e\rangle$  and  $|g\rangle$  states.

put can be effectively controlled by several key parameters, including the control field intensity ( $\Omega_c$ ), the atom–cavity coupling strength ( $g$ ), and the cavity decay rate ( $\kappa$ ). Among these parameters, the control field intensity,  $\Omega_c$ , represents an experimentally accessible degree of freedom, whereas the others are largely determined by the cavity geometry, mirror reflectivity, and the choice of atomic energy levels. As a result, parameters such as  $g$  and  $\kappa$  cannot be easily tuned under typical experimental constraints, whereas  $\Omega_c$  can be easily modified by tweaking the laser power. As the control field intensity  $\Omega_c$  increases, the full width at half maximum (FWHM) of the EIT resonance also increases significantly, typically by approximately 10 kHz. This is the key on which the ion thermometry method is further established.

For the purpose of ion thermometry, it is essential to include the vibrational levels associated with each relevant electronic energy level. Addressing these vibrational states requires operation in the resolved-sideband regime ( $\gamma \ll \omega_{sec}$ ) [1, 31], where the splitting between adjacent vibrational levels,  $\hbar\omega_{sec}$ , exceeds the natural linewidth of the corresponding transition,  $2\gamma$ . Here,  $\gamma$  denotes the spontaneous decay

rate of the transition, and  $\omega_{sec}$  represents the secular frequency of the trapped ion.

Henceforth, a transition between two energy levels refers to a transition between their corresponding vibrational states. The allowed transitions can be classified into three main types: the carrier transition, the blue sideband (BSB) transition, and the red sideband (RSB) transition, corresponding to  $\Delta n = 0$  and  $\Delta n = \pm 1$ , respectively. The vibrational level occupancy,  $n$ , directly influences the ion–field coupling strength when sideband transitions are addressed. Consequently, the Rabi frequencies for the RSB and BSB transitions are modified as [1],

$$\Omega_{\text{BSB}} = \Omega_0 \sqrt{n+1}, \quad (1)$$

$$\Omega_{\text{RSB}} = \Omega_0 \sqrt{n}.$$

In contrast, for the carrier transition, the Rabi frequency remains unchanged ( $\Omega_0$ ). When the control laser is tuned to a sideband transition (BSB or RSB), the effect of the phonon occupancy,  $n$ , becomes evident in the EIT linewidth through its influence on the Rabi frequency,  $\Omega_c$ . Conversely, variations in the EIT linewidth provide an estimate of changes in the ion’s vibrational occupancy. Motivated by this relationship, we investigate this phenomenon

through numerical simulations and identify a systematic approach to estimate the ion temperature, which is directly linked to the phonon occupancy.

We consider a  $\Lambda$ -type three-level system confined inside a high-finesse optical cavity. The states are considered to be coupled with vibrational state, denoted by  $|u, n\rangle$ ,  $|e, n+1\rangle$ , and  $|g, n\rangle$ . The cavity mode couples to the atomic transition  $|g, n+1\rangle \leftrightarrow |e, n+1\rangle$  with coupling strength  $g$ , while a classical control laser couples the transition  $|u, n\rangle \leftrightarrow |g, n+1\rangle$  by a change in single quanta of the phonon mode with Rabi frequency  $\Omega_c$  (see Figure 1b). A weak input probe field of amplitude  $\epsilon$  and frequency  $\omega_{\text{probe}}$  is applied at  $\Delta$  detuning. The  $\Delta$  is changed both side of resonance to obtain the cavity output. The spontaneous decay rates from level  $|e, n+1\rangle \rightarrow |u, n+1\rangle$  and  $|e, n+1\rangle \rightarrow |g, n+1\rangle$  are  $\gamma_{eu}$  and  $\gamma_{eg}$  respectively.

We operate in the Lamb-Dicke regime ( $\eta \ll 1$ ), where the control laser and ion's motion can be expanded to first order in the Lamb-Dicke parameter  $\eta$ . Operators  $b$  and  $b^\dagger$  describe phonon-assisted transitions, achieved by tuning the coupling laser to the first motional sideband of the  $|u\rangle \leftrightarrow |e\rangle$  transition [1].

In a frame rotating at the probe frequency  $\omega_{\text{probe}}$ , and under the electric dipole and rotating-wave approximations (RWA), the time-independent Hamiltonian for the atom-cavity system is given by (with  $\hbar = 1$ ):

$$H = \Delta_p \sigma_{gg} - \Delta_p a^\dagger a + g (a^\dagger \sigma_{ge} + a \sigma_{eg}) + \eta \Omega_c (\sigma_{eu} b^\dagger + \sigma_{ue} b) + \epsilon (a^\dagger + a). \quad (2)$$

where,  $\sigma_{ij} = |i\rangle \langle j|$  are the atomic transition operators. The detuning parameter  $\Delta_p = \omega_{\text{probe}} - \omega_{31}$  represents the frequency mismatch between the probe laser and the atomic transition  $|g, n+1\rangle \leftrightarrow |e, n+1\rangle$ .

The first term of the Hamiltonian describes the energy of the atomic state  $|g, n+1\rangle$  in the

rotating frame, while the second term corresponds to the energy of the cavity photons. The cavity field is described by photon annihilation ( $a$ ) and creation ( $a^\dagger$ ) operators.

The third term accounts for the coherent interaction between the cavity field and the atomic transition  $|g, n+1\rangle \leftrightarrow |e, n+1\rangle$ . ( $b$ ) and ( $b^\dagger$ ) are phonon annihilation and creation operators respectively. The fourth term describes the interaction between the atomic transition  $|e, n+1\rangle \leftrightarrow |u, n+1\rangle$  and the vibrational mode of the ion, mediated by the control laser. The last term represents the coherent drive applied to the cavity field by the pump laser.

The open dynamics follow the Lindblad master equation [32],

$$\frac{d\rho}{dt} = -i [H, \rho] + \mathcal{L}_{\text{cav}}[\rho] + \mathcal{L}_{\text{atom}}[\rho] + \mathcal{L}_{\text{ph}}[\rho], \quad (3)$$

with cavity loss

$$\mathcal{L}_{\text{cav}}[\rho] = \kappa (2a\rho a^\dagger - a^\dagger a\rho - \rho a^\dagger a), \quad (4)$$

where  $\kappa$  denotes the decay rate of the cavity field.

The spontaneous emission from the excited atomic state  $|3\rangle$  to the lower states  $|j\rangle$  ( $j = 1, 2$ ) is given by

$$\mathcal{L}_{\text{atom}}[\rho] = \sum_{j=1,2} \gamma_{3j} (2\sigma_{j3}\rho\sigma_{3j} - \sigma_{33}\rho - \rho\sigma_{33}), \quad (5)$$

where  $\gamma_{3j}$  represents the spontaneous decay rate from state  $|e\rangle$  to state  $|j\rangle$ .

The phonon states are inherent to damping due to fluctuating electric field noise present in real ion trap. To account this scenario we considered the trapped ion system such that it is coupled to a thermal bath. The fluctuation causes, initially the phonon numbers to be exchanged between the ion and reservoir, attending an equilibrium condition. The damping of the vibrational mode of the ion due to its coupling with a thermal reservoir is described by [6]

$$\mathcal{L}_{\text{ph}}[\rho] = \gamma_b (n_{\text{th}} + 1) (2b\rho b^\dagger - b^\dagger b\rho - \rho b^\dagger b) + \gamma_b n_{\text{th}} (2b^\dagger \rho b - b b^\dagger \rho - \rho b b^\dagger), \quad (6)$$

where  $\gamma_b$  is the phonon damping rate and  $n_{th}$  denotes the mean thermal phonon number at equilibrium. The average phonon number ( $\bar{n}$ ) is related to temperature of the ion by,

$$\bar{n} = \frac{1}{\exp(\hbar\omega_{osc}/k_b T) - 1} \quad (7)$$

Following Equation 6 the rate equation for phonon can be derived as [6],

$$\dot{\bar{n}}(t) = -\gamma_b \bar{n}(t) + \gamma_b n_{th} \quad (8)$$

So, close to ground state ( $\bar{n} = 0$ ),  $\dot{\bar{n}}(t) = \gamma_b n_{th}$ . This gives an initial estimation of heating rate of the ion. Equation 8, also shows that if a long time interval is taken, i.e. at equilibrium,  $\bar{n}_{eq} = n_{th}$ . So, determining the value of  $n_{th}$  allows us to estimate the ion's temperature owing to Equation 7.

### III. ANALYSIS OF TRANSMISSION IN CAVITY-EIT

We numerically solve the master equation (Equation 3) using the Hamiltonian given in Equation 2. The probe-field detuning is varied across the resonance, and the steady-state density matrix is obtained for each detuning value. From the steady-state solution, the photon buildup inside the cavity is extracted by evaluating the expectation value of the photon number operator,  $\langle a^\dagger a \rangle$ . Multiplying the intra-cavity photon number by the cavity decay rate,  $\kappa$ , yields the cavity output, or the cavity-EIT spectrum (see Figure 2). This spectrum exhibits the characteristic features of previously reported cavity-EIT systems [16, 17, 24, 33].

The cavity linewidth is observed to be narrower than that of an empty cavity, and the vacuum Rabi splitting peaks appear at  $\Delta = \pm\sqrt{g^2 + \Omega_c^2}$ . For all simulations presented in this work, unless otherwise stated, the system parameters are fixed as follows. All quantities are normalized with respect to the cavity decay rate,  $\kappa$ , which is taken to be 0.4 MHz, a typical value for a high-finesse cavity. The coupling-field Rabi frequency,  $\Omega_c$ , is set to  $2.5\kappa$ , while the

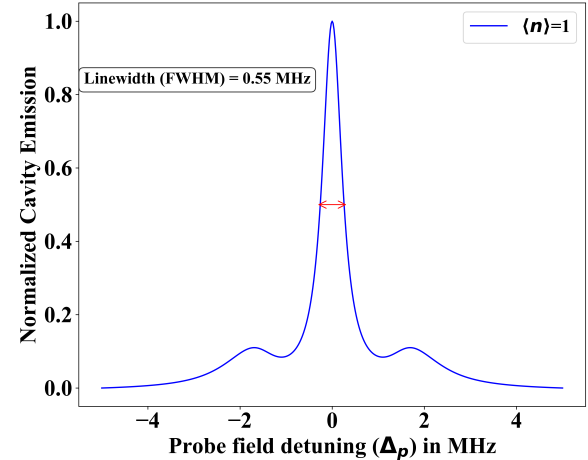


FIG. 2: Simulated cavity-EIT transmission spectrum for  $\kappa = 0.4$  MHz,  $g = 3\kappa$ ,  $\gamma_{eg} = \gamma_{eu} = \kappa$ ,  $\langle n \rangle = 1$ , and  $\gamma_b = 0.25\kappa$ . The observed linewidth (0.55 MHz) is narrower than the empty cavity linewidth  $2\kappa = 0.8$  MHz. The vacuum Rabi splitting peaks occur at  $\pm\sqrt{g^2 + \Omega_c^2} = \pm 1.56$  MHz.

atom-cavity coupling strength,  $g$ , is chosen as  $3\kappa$ . The decay rates from the excited states,  $\gamma_{ge}$  and  $\gamma_{ue}$ , are taken to be equal to  $\kappa$ . In addition, motional-state decoherence is included to account for unwanted heating or cooling of the ion arising from phase noise and radiative fluctuations present in realistic ion traps. To model this effect, a weak coupling between the motional state and the environment is introduced, characterized by a coupling constant  $\gamma_b \approx 0.25\kappa$ .

### IV. EFFECT OF THERMAL STATE ON CAVITY EIT LINEWIDTH

The usual cavity-EIT formalism discussed in the literature does not explicitly include the ion's motional state. This inherently makes an assumption that the ion is fixed in space and the effect of ion thermalization doesn't affect the cavity-EIT output. When the ion's motion is not considered for cavity based EIT the Hamiltonian is simplified to,

$$H_{EIT} = \Delta_p \sigma_{gg} - \Delta_p a^\dagger a + g (a^\dagger \sigma_{ge} + \sigma_{eg} a) + \Omega_c (\sigma_{ue} + \sigma_{eu}) + \varepsilon (a^\dagger + a) \quad (9)$$

Where the different terms have their usual

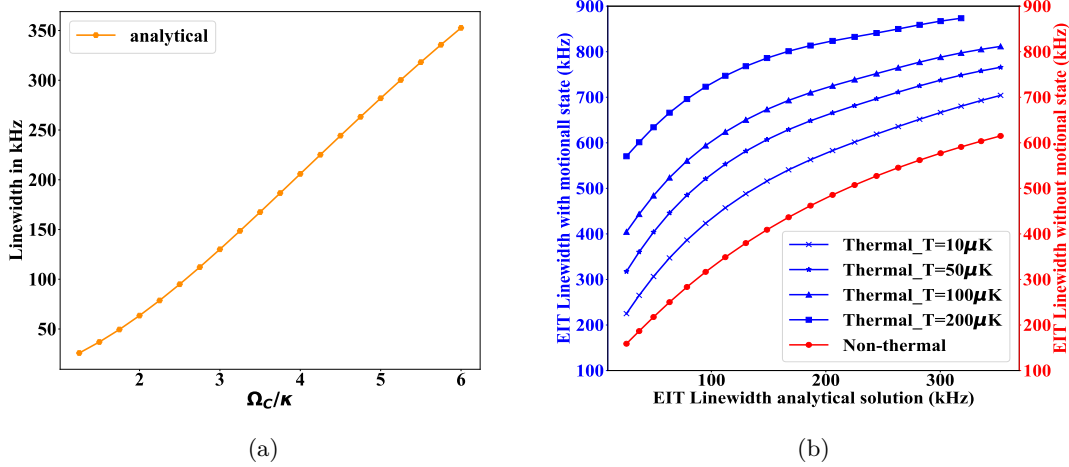


FIG. 3: (a) Cavity-EIT linewidth from analytical expression as a function of control field Rabi frequency. (b) Comparison of linewidth without considering motional state vs with motional state for different temperatures of ion. The parameters for the plots chosen as follows,  $\kappa = 0.4\text{MHz}$ ,  $g = 3\kappa$ ,  $\gamma_{eg} = \gamma_{eu} = \kappa$ ,  $\gamma_b = 0.04\kappa$ .

meaning as described in section II. We refer this formalism as non-thermal and the Hamiltonian given in Equation 9, the non-thermal cavity-EIT Hamiltonian. The output of the cavity is traced from the average of photon number operator with the variation of the probe field detuning. The same cavity transmission can also be analytically calculated from the expression[34],

$$T = \frac{\kappa^2}{|(\Delta_p + i\kappa) - g^2 N \chi|^2} \quad (10)$$

Where,

$$\chi = g^2 N \frac{\Delta_p}{(\Delta_p + i(\gamma_{eu} + \gamma_{eg})\Delta_p - \frac{1}{4}\Omega_c^2)} \quad (11)$$

The linewidth depends on the effective Rabi coupling,  $\Omega_c$ , exhibiting power-broadening behavior. In Figure 3a, the relationship between the effective Rabi coupling and the cavity-EIT linewidth is shown using the analytical expression.

When the motional states are incorporated into the Hamiltonian (Equation 2), providing a more general description of a trapped ion, the cavity-EIT linewidth deviates from the non-thermal case. As the temperature increases, the thermal nature of the ion leads to a higher motional occupancy. This increase in motional oc-

cupation modifies the cavity-EIT linewidth by changing  $\Omega_c$ , as discussed in detail in section II.

To compare the linewidths in the thermal and non-thermal cases, we perform simulations for both scenarios using the same values of  $\Omega_c$  as those employed in the analytical plot in Figure 3a. The thermal simulations are carried out over a range of temperatures to capture the dependence of the cavity linewidth on the ion temperature. In Figure 3b, the thermal and non-thermal linewidths are presented, with the analytical linewidths from Figure 3a used as the reference on the x-axis.

We observe that, over the entire range, the non-thermal linewidth remains lower than the thermal linewidth, and that the linewidth curves shift toward higher values as the temperature increases. This behavior provides further motivation for quantifying the ion temperature, as it modifies the cavity linewidth, which is highly sensitive to temperature-induced changes in the ion's motional state.

## V. DETERMINATION OF ION TEMPERATURE AND AVERAGE PHONON NUMBER

We studied this cavity-EIT phenomenon with the motivation of determining the ion temper-

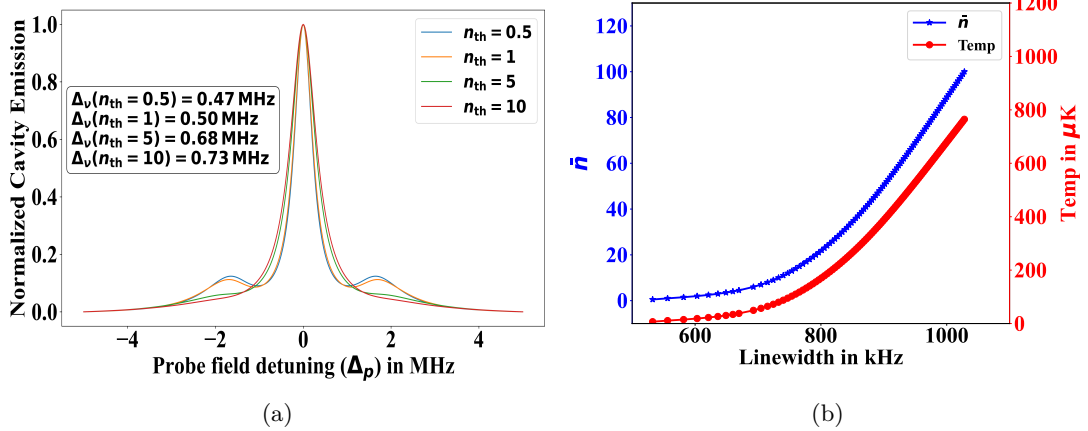


FIG. 4: (a) Cavity-EIT spectrum for different  $n_{th}$  value (b) Ion temperature and average phonon occupancy ( $\bar{n}$ ) as a function of cavity-EIT linewidth. Parameters used are:  $\kappa = 0.4\text{MHz}$ ,  $g = 3\kappa$ ,  $\gamma_{eg} = \gamma_{eu} = \kappa$ ,  $n_{th} = \langle n \rangle = 1$ ,  $\gamma_b = 0.25\kappa$ .

ature. It is evident from section IV that the linewidth of the cavity-EIT spectrum appears to serve as a probe parameter for temperature. The ion-temperature is incorporated in the systems by means of the thermal bath phonon occupancy ( $n_{th}$ ) following Equation 7 and Equation 8 in steady state.

The simulation is performed for four different values of the thermal bath phonon occupancy,  $n_{th} = 0.5, 1, 5$ , and  $10$ , using the same set of parameters described in section III. A clear trend of increasing linewidth with increasing  $n_{th}$  is observed (see Figure 4a). This behavior indicates that the ion temperature can be mapped to the observed cavity-EIT linewidth. In other words, by analyzing the EIT width of the cavity-EIT spectrum, the ion temperature can be inferred.

In addition, the average phonon occupancy,  $\bar{n}$ , is an important quantity for various applications, such as estimating heating rates, determining fidelity of ion trap based quantum gates, indicating Lamb-Dicke regime etc. Since the phonon occupancy is directly related to temperature (see Equation 7),  $\bar{n}$  can also be estimated from the cavity-EIT linewidth.

We further perform simulations over a wide range of ion temperatures, from which the

linewidth is calculated by fitting a lorentzian function to the spectrum. The average phonon occupancy  $\bar{n}$  is extracted by taking the expectation over phonon number operator ( $\langle b^\dagger b \rangle$ ). In Figure 4b, the ion temperature and  $\bar{n}$  are illustrated as functions of the cavity-EIT linewidth. The predicted temperature exhibits an asymptotic behavior at low linewidth values, indicating that at very low temperatures, variations in linewidth are minimal.

This behavior can be understood from the  $\sqrt{n}$  dependence of the control field Rabi frequency,  $\Omega_c$ , which directly governs the cavity-EIT linewidth. At low temperatures, small changes in temperature lead to rapid variations in  $\Omega_c$ , as described by Equation 1, resulting in noticeable changes in the linewidth. In contrast, at higher temperatures, the linewidth tends to saturate because variations in  $\Omega_c$  become negligible.

The average phonon occupation,  $\bar{n}$ , follows a similar trend to the temperature as the cavity-EIT linewidth changes. This behavior arises from the approximately linear relationship between  $\bar{n}$  and temperature derived from Equation 7, given by

$$\bar{n} \approx \frac{k_B T}{\hbar \omega} \quad (12)$$

Further, we demonstrate how the atom-

cavity coupling strength affects the cavity-EIT linewidth,  $g$ , and Rabi frequency of the coupling laser. We provide linewidth maps in two dimensions for a range of mean thermal phonon number values. Appendix A contains the relevant plots.

## VI. ROADMAP TOWARDS EXPERIMENTAL REALIZATION

We present here an outline of experimentally implementing the trapped-ion thermometry method presented in this paper. As the thermal state detection method proposed is cavity EIT-based, one needs to engineer a trapped-ion cavity-QED system in the strong-coupling regime ( $g^2 \gg \kappa\gamma$ ). The cavity configuration may be chosen to be concentric or confocal as per the requirements of the physics objectives. We recommend using a high finesse ( $> 50000$ ) cavity, such that the coupling factor ( $g$ ) is high enough to justify operation in the strong coupling regime ( $g^2 \gg \kappa\gamma$ ).

We need to choose a particular ion-species with suitable energy levels, and appropriate ion trap parameters such that the system stays in the resolved sideband regime ( $\gamma \ll \omega_{sec}$ ). Most of the ion species used in cavity qed experiments globally typically have strong dipole-allowed transitions, with broad linewidths, where sidebands are not resolved in general. Such traps operate with typical trap frequencies in the range ( $\omega_{sec}$ )  $\approx 0.5 - 2 MHz$ . So, one needs a judicious choice of the energy levels, such that the effective three-level system realized has very narrow linewidths for one of the excited levels.

One may also consider using a dipole allowed transition (where typical linewidths are in the range of  $\approx 5 - 20 MHz$ ) for the trapped ion strongly coupled to the cavity field, one should consider operating the ion trap in a very tight confinement (very deep trap potential) of the ion with secular frequency greater transition linewidth ( $\Gamma$ ). Such a mode of ion trap operation has been experimentally validated [35], where an  ${}^9Be^+$  ion was trapped with a very high RF voltage (600 V) and frequency (240 MHz), reaching secular frequencies in the range of  $\sim 50 MHz$

and the sideband transitions were addressed in a dipole allowed transition .

## VII. CONCLUSION

We have presented a cavity-assisted thermometry scheme for trapped ions that takes advantage of the dependence of cavity-induced EIT on ions' motional state. Through the explicit integration of thermalization and vibrational sidebands into a cavity-QED  $\Lambda$ -type system, we show that the mean phonon occupation and the ion temperature can be directly measured by the linewidth of the cavity-EIT transparency window. By means of motion-induced dephasing, thermal phonons perturb the coherence of the EIT dark state, resulting in a systematic expansion of the cavity-EIT resonance. This effect allows temperature readout directly from the cavity transmission spectrum, eliminating the need for projective internal-state detection in Rabi spectroscopy. Overall, for the diagnosis of ion temperature in cavity-QED systems, cavity-EIT-based thermometry provides a minimally invasive and experimentally feasible method. The established coupling between ion motion and cavity transmission goes beyond thermometry, offering a platform to investigate measurement-induced effects in cavity-QED systems and enabling continuous monitoring of motional heating.

## Acknowledgments

Abhijit Kundu gratefully acknowledges financial support from IIT Tirupati, Government of India. Vijay Bhatt acknowledges support from the NQM (National Quantum Mission), Department of Science and Technology, Ministry of Science and Technology, Government of India through Project No. DST/QTC/NQM/QComm/2024/2(G) administered through the IITM CDOT SAMGYNA TECHNOLOGIES FOUNDATION, IIT Madras, Chennai, Tamil Nadu - 600113. Arijit Sharma acknowledges support from the NQM (National Quantum

Mission), Department of Science and Technology, Ministry of Science and Technology, Government of India through Project Nos. DST/QTC/NQM/QComm/2024/2(G) and DST/QTC/NQM/QComm/2024/2(C) administered through the IITM CDOT SAMG-

YNA TECHNOLOGIES FOUNDATION, IIT Madras, Chennai, Tamil Nadu - 600113.

### Conflicts of Interest

The authors declare no conflicts of interest.

---

[1] D. Leibfried, R. Blatt, C. Monroe, and D. Wineland, Quantum dynamics of single trapped ions, *Rev. Mod. Phys.* **75**, 281 (2003).

[2] H. Häffner, C. F. Roos, and R. Blatt, Quantum computing with trapped ions, *Phys. Rep.* **469**, 155 (2008).

[3] C. Monroe and J. Kim, Scaling the ion trap quantum processor, *Science* **339**, 1164 (2013).

[4] D. Fang, W.-B. Chen, C.-H. Zhang, J.-M. Cui, Y.-F. Huang, C.-F. Li, and G.-C. Guo, Cavity-assisted thermometry for a single trapped ion, *Phys. Rev. Appl.* **24**, 024037 (2025).

[5] D. J. Wineland, C. Monroe, W. M. Itano, D. Leibfried, B. E. King, and D. M. Meekhof, Experimental issues in coherent quantum-state manipulation of trapped atomic ions, *J. Res. Natl. Inst. Stand. Technol.* **103**, 259 (1998).

[6] M. Brownnutt, M. Kumph, P. Rabl, and R. Blatt, Ion-trap measurements of electric-field noise near surfaces, *Rev. Mod. Phys.* **87**, 1419 (2015).

[7] F. Diedrich, J. C. Bergquist, W. M. Itano, and D. J. Wineland, Laser cooling to the zero-point energy of motion, *Phys. Rev. Lett.* **62**, 403 (1989).

[8] C. F. Roos, D. Leibfried, A. B. Mundt, F. Schmidt-Kaler, J. Eschner, and R. Blatt, Experimental demonstration of ground state laser cooling with electromagnetically induced transparency, *Phys. Rev. Lett.* **85**, 5547 (2000).

[9] D. M. Meekhof, C. Monroe, B. E. King, W. M. Itano, and D. J. Wineland, Generation of nonclassical motional states of a trapped atom, *Phys. Rev. Lett.* **76**, 1796 (1996).

[10] C. Roos, T. Zeiger, H. Rohde, H. C. Nägerl, J. Eschner, D. Leibfried, F. Schmidt-Kaler, and R. Blatt, Quantum state engineering on an optical transition and decoherence in a paul trap, *Phys. Rev. Lett.* **83**, 4713 (1999).

[11] A. J. Rasmussen, M. D'Onofrio, Y. Xie, J. Cui, and P. Richerme, Optimized pulsed sideband cooling and enhanced thermometry of trapped ions, *Phys. Rev. A* **104**, 043108 (2021).

[12] I. Vybornyi, L. S. Dreissen, D. Kiesenhofer, H. Hainzer, M. Bock, T. Ollikainen, D. Vadlejch, C. F. Roos, T. E. Mehlstäubler, and K. Hammerer, Sideband thermometry of ion crystals, *PRX Quantum* **4**, 040346 (2023).

[13] V. M. Acosta, K. Jensen, C. Santori, D. Budker, and R. G. Beausoleil, Electromagnetically induced transparency in a diamond spin ensemble enables all-optical electromagnetic field sensing, *Phys. Rev. Lett.* **110**, 213605 (2013).

[14] H. Wang, D. Goorskey, W. Burkett, and M. Xiao, Cavity linewidth narrowing by means of electromagnetically induced transparency, *Opt. Lett.* **25**, 1732 (2000).

[15] M. J. Werner and A. Imamoğlu, Photon-photon interactions in cavity electromagnetically induced transparency, *Phys. Rev. A* **61**, 011801 (1999).

[16] M. Mücke, E. Figueroa, J. Bochmann, C. Hahn, K. Murr, S. Ritter, C. J. Villas-Boas, and G. Rempe, Electromagnetically induced transparency with single atoms in a cavity, *Nature* **465**, 755 (2010).

[17] H. Tanji-Suzuki, W. Chen, R. Landig, J. Simon, and V. Vuletić, Vacuum-induced transparency, *Science* **333**, 1266 (2011).

[18] L.-M. Duan and C. Monroe, Colloquium: Quantum networks with trapped ions, *Rev. Mod. Phys.* **82**, 1209 (2010).

[19] A. Reiserer, Colloquium: Cavity-enhanced quantum network nodes, *Rev. Mod. Phys.* **94**, 041003 (2022).

[20] K.-J. Boller, A. Imamoğlu, and S. E. Harris, Observation of electromagnetically induced transparency, *Phys. Rev. Lett.* **66**, 2593 (1991).

[21] I. Novikova, R. L. Walsworth, and Y. Xiao, Electromagnetically induced transparency-based slow and stored light in warm atoms, *Laser Photonics Rev.* **6**, 333 (2012).

[22] L. Ma, O. Slattery, and X. Tang, Optical quantum memory based on electromagnetically induced transparency, *J. Opt.* **19**, 043001 (2017).

[23] G. Morigi, J. Eschner, and C. H. Keitel, Ground state laser cooling using electromagnetically induced transparency, *Phys. Rev. Lett.* **85**, 4458 (2000).

[24] J. Souza, E. Figueroa, H. Chibani, C. Villas-Boas, and G. Rempe, Coherent control of quantum fluctuations using cavity electromagnetically induced transparency, *Phys. Rev. Lett.* **111**, 113602 (2013).

[25] J. I. Cirac, R. Blatt, P. Zoller, and W. D. Phillips, Laser cooling of trapped ions in a standing wave, *Phys. Rev. A* **46**, 2668 (1992).

[26] M. D. Lukin, M. Fleischhauer, M. O. Scully, and V. L. Velichansky, Intracavity electromagnetically induced transparency, *Opt. Lett.* **23**, 295 (1998).

[27] H. Wu, J. Gea-Banacloche, and M. Xiao, Observation of intracavity electromagnetically induced transparency and polariton resonances in a doppler-broadened medium, *Phys. Rev. Lett.* **100**, 173602 (2008).

[28] J. Zhang, G. Hernandez, and Y. Zhu, Slow light with cavity electromagnetically induced transparency, *Opt. Lett.* **33**, 46 (2007).

[29] M. Albert, A. Dantan, and M. Drewsen, Cavity electromagnetically induced transparency and all-optical switching using ion coulomb crystals, *Nat. Photon.* **5**, 633 (2011).

[30] Y.-C. Liu, B.-B. Li, and Y.-F. Xiao, Electromagnetically induced transparency in optical microcavities, *Nanophotonics* **6**, 789 (2017).

[31] S. Zhang, Z.-P. Huang, T.-C. Tian, Z.-Y. Wu, J.-Q. Zhang, W.-S. Bao, and C. Guo, Sideband cooling of a

trapped ion in strong sideband coupling regime, Opt. Express **31**, 44501 (2023).

[32] D. Manzano, A short introduction to the Lindblad master equation, AIP Adv. **10**, 025106 (2020).

[33] L. R. S. Santos, M. H. Oliveira, L. O. R. Solak, D. Z. Rossatto, and C. J. Villas-Boas, Fundamental limit to cavity linewidth narrowing with single atoms (2024), arXiv:2411.12422 [quant-ph].

[34] M. Mücke, *Elektromagnetisch induzierte Transparenz mit einem einzelnen Atom*, Ph.D. thesis, Technische Universität München (2011).

[35] S. R. Jefferts, C. Monroe, E. W. Bell, and D. J. Wineland, Coaxial-resonator-driven rf (paul) trap for strong confinement, Phys. Rev. A **51**, 3112 (1995).

[36] Q. A. Turchette, Kielpinski, B. E. King, D. Leibfried, D. M. Meekhof, C. J. Myatt, M. A. Rowe, C. A. Sackett, C. S. Wood, W. M. Itano, C. Monroe, and D. J. Wineland, Heating of trapped ions from the quantum ground state, Phys. Rev. A **61**, 063418 (2000).

[37] E. Peik, J. Abel, T. Becker, J. von Zanthier, and H. Walther, Sideband cooling of ions in radio-frequency traps, Phys. Rev. A **60**, 439 (1999).

#### Appendix A: Dependency of cavity-EIT linewidth on cavity coupling parameter $g$ and control field Rabi frequency, $\Omega_c$ for different $n_{th}$

A two-dimensional map of the cavity-EIT linewidth represented as the normalized full width at half maxima (FWHM) ratio as a function of the normalized control field Rabi frequency  $\Omega_c$  and the normalized atom-cavity coupling strength  $g$  for various mean thermal phonon numbers  $n_{th}$  is shown in Figure 5. For a weakly excited motional state ( $n_{th} = 0.5$ ) (see Figure 5a), the linewidth ratio remains close to unity over a large region of the parameter space. This suggests that thermal motion only slightly alters EIT coherence. As the value of thermal occupation increases  $n_{th} = 1$  (see Figure 5b), a clear reduction of the FWHM ratio occurs, particularly in the regime of strong ion-cavity coupling and weak control fields. This reduction signals the onset of thermally induced decoherence. A higher phonon number ( $n_{th} = 5, 10$ ) (see Figure 5c, Figure 5d) shows a more noticeable trend in which the parameter space is dominated by extended regions of reduced linewidth ratio. In this regime, thermal motion significantly perturbs the ion-cavity interaction, leading to enhanced dephasing and a degradation of the EIT interference.

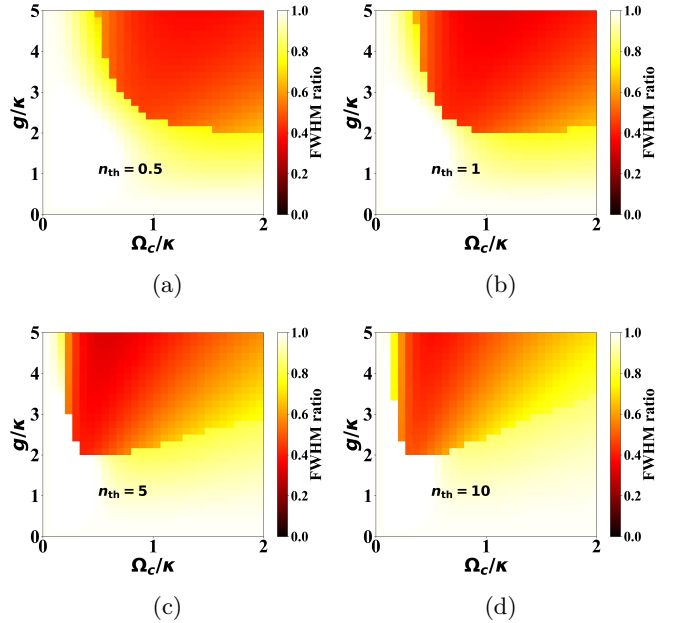


FIG. 5: Two-dimensional maps of the cavity-EIT linewidth as a function of the atom-cavity coupling strength  $g$  and the coupling-laser Rabi frequency  $\Omega_c$  for different mean thermal phonon numbers  $\bar{n}_{th}$ .

As the control-field strength increases, it partially mitigates this effect by stabilizing the dark state against motional fluctuations. The strong sensitivity of the cavity response to the ions motional state is highlighted by the systematic and temperature-dependent modification of the cavity-EIT linewidth shown in these plots. This provide a solid foundation for thermometry using cavity-based EIT.

#### Appendix B: Verification of different sideband transition related phenomenon

As a proof of principle of our approach, we performed verification of different sideband transition related characteristics. In case of sideband transitions, a two-level system dressed with vibrational levels is sufficient to address different properties. The sideband Hamiltonians used here are consistent with the Lamb-Dicke-expanded interaction employed in the main text. The two kinds of sideband transitions (BSB and RSB) are described by the Hamiltonian which is similar to the 4th term (with the multiplication of the Lamb-Dicke parameter  $\eta$ ) of Equation 2 with the reduced Hilbert space of only photon

and phonon. The Hamiltonian for blue and red sideband transition can be written as [1],

$$\begin{aligned} H_{BSB} &= \eta\Omega_c (\sigma_{eu}b^\dagger + \sigma_{ue}b) \\ H_{RSB} &= \eta\Omega_c (\sigma_{eu}b + \sigma_{ue}b^\dagger) \end{aligned} \quad (\text{B1})$$

For a thermal distribution of ion the strengths of red and blue sideband transitions are unequal and depends on the phonon number ( $n$ ). The probability of occupying the excited state for RSB and BSB transition is related by the formula [36],

$$\frac{P_{RSB}}{P_{BSB}} = \frac{n}{n+1} \quad (\text{B2})$$

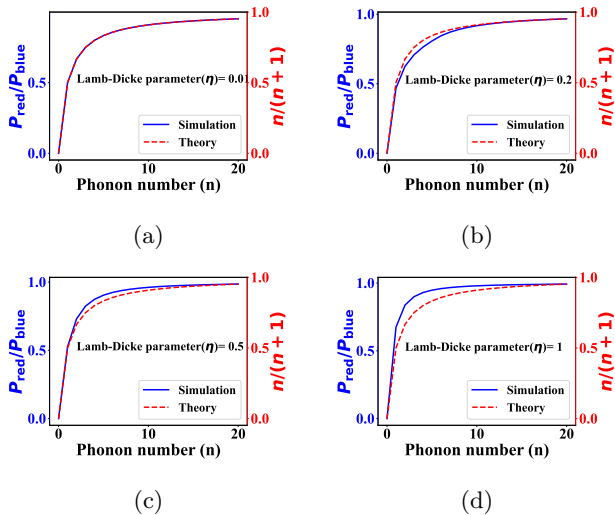


FIG. 6: Ratio of excited state occupation probability for blue and red sideband transition is compared with phonon number ratio. Plots (a)–(d) correspond to increasing values of the Lamb–Dicke parameter  $\eta$ .

We verified this principle for a range of phonon numbers and different Lamb-Dicke parameters. In Figure 6, the comparison between the probability ratio from simulation and phonon ratio from Equation B2 has been shown for four different Lamb-Dicke parameters. At lower values of Lamb-Dicke parameters, these two quantities are well-matched, which consistent with the theory. For higher Lamb-Dicke parameters the simulation result and theory starts to deviate as the boundary of Lamb-Dicke regime ( $\eta \ll 1$ ) is approached, whereas sideband transitions assume that the ion is well within the Lamb-Dicke Regime.

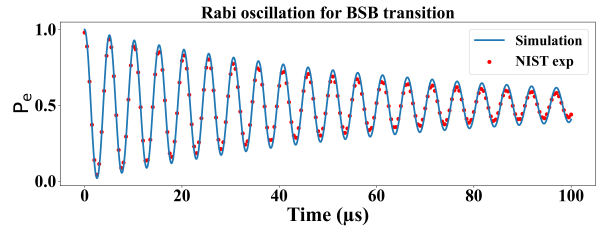


FIG. 7: Rabi oscillation in Blue sideband transition for  $n = 0 \rightarrow 1$ . The red dots represent the data from the NIST experiment [9], and the solid blue line shows the simulation result for the same set of parameters used in the experiment. The parameters are,  $\eta = 0.202$ ,  $\Omega = 2\pi \times 500$  kHz,  $\gamma = 20$  kHz.

The dephasing and frequency in the Rabi oscillation of the blue sideband transition depend on the phonon occupation. There are many experimental verifications for this phenomenon [5, 9]. We have verified this argument and matches with the experimental data reported in the NIST experiment (see Figure 7) [9].

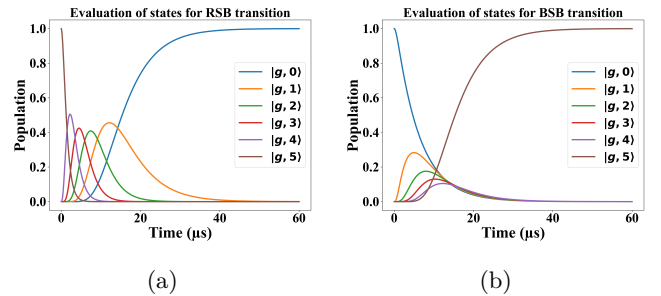


FIG. 8: Simulated state evolution with time. The simulation runs with Lamb-Dicke parameter,  $\eta = 0.2$ , Rabi frequency,  $\Omega = 2\text{MHz}$ , and excited state decay rate,  $\gamma = 2\Omega$ . (a) Time evolution of different states in red sideband transition. The initial state is taken as  $|g, 5\rangle$ , after applying sequential RSB pulses, phonon number decreases, and finally the system reaches the ground state,  $|g, 0\rangle$ . (b) Time evolution for blue sideband transition. population goes from initial  $|g, 0\rangle$  to higher phonon state  $|g, 5\rangle$ .

A larger application of the sideband transition is the cooling of the atom to its motional ground state [7, 37]. When the resolved sideband regime is obtained ( $\gamma \ll \omega_{sec}$ ) and the laser is tuned to a RSB transition, the atom loses one quanta of energy upon excitation ( $|g, n\rangle \rightarrow |e, n-1\rangle$ ). From the excited state, there is a high chance that it spontaneously decays to the ground state with

the same motional quanta ( $|g, n - 1\rangle$ ). Thus, a motional quanta has been reduced in this process. By repeating this process multiple times, the vibrational quanta has been reduced in each steps and eventually we reached to the ground

state of the atom (see Figure 8a). Similarly, if the laser is tuned to the BSB transition, starting from a ground state, the atom lands in a higher phonon state depending on the number of side-band pulses applied (see Figure 8b).